


Nonlocal Exciton-Photon Interactions in Hybrid High- Q Beam Nanocavities with Encapsulated MoS₂ Monolayers

Chenjiang Qian^{1,*}, Viviana Villafañe¹, Pedro Soubelet¹, Alexander Hötger¹, Takashi Taniguchi², Kenji Watanabe³, Nathan P. Wilson¹, Andreas V. Stier¹, Alexander W. Holleitner¹, and Jonathan J. Finley^{1,†}

¹Walter Schottky Institut and Physik Department, Technische Universität München, Am Coulombwall 4, 85748 Garching, Germany

²International Center for Materials Nanoarchitectonics, National Institute for Materials Science, 1-1 Namiki, Tsukuba 305-0044, Japan

³Research Center for Functional Materials, National Institute for Materials Science, 1-1 Namiki, Tsukuba 305-0044, Japan

 (Received 8 July 2021; revised 11 February 2022; accepted 24 May 2022; published 10 June 2022)

Atomically thin semiconductors can be readily integrated into a wide range of nanophotonic architectures for applications in quantum photonics and novel optoelectronic devices. We report the observation of nonlocal interactions of “free” trions in pristine hBN/MoS₂/hBN heterostructures coupled to single mode ($Q > 10^4$) quasi 0D nanocavities. The high excitonic and photonic quality of the interaction system stems from our integrated nanofabrication approach simultaneously with the hBN encapsulation and the maximized local cavity field amplitude within the MoS₂ monolayer. We observe a nonmonotonic temperature dependence of the cavity-trion interaction strength, consistent with the nonlocal light-matter interactions in which the extent of the center-of-mass (c.m.) wave function is comparable to the cavity mode volume in space. Our approach can be generalized to other optically active 2D materials, opening the way toward harnessing novel light-matter interaction regimes for applications in quantum photonics.

DOI: [10.1103/PhysRevLett.128.237403](https://doi.org/10.1103/PhysRevLett.128.237403)

Monolayer crystals of transition metal dichalcogenides (TMDs) are ideally suited as the active material for solid-state cavity quantum electrodynamics (cQED) investigations [1,2]. They have very large exciton binding energies ≥ 100 meV [3,4], linewidths close to the homogeneous limit when suitably encapsulated by hexagonal boron nitride (hBN) [5–7], and strong optical absorption strengths close to the excitonic transitions exceeding $\sim 10\%$ per atomically thin layer [8]. In addition, 2D materials can be readily attached to a wide range of substrates [9], making them ideally suited for hybrid solid-state cQED experiments [10]. Indeed, recent work has reported strong light-matter coupling for monolayer TMDs using diverse photonic resonator geometries including planar open-fiber cavities [11], photonic crystals [12–14], and nanoplasmonic Tamm resonators [15–17]. However, the direct coupling of 2D semiconductors to quasi 0D nanophotonic modes while preserving excellent excitonic properties and high cavity quality (Q) factor has remained a challenge. Most commonly, nonencapsulated TMD monolayers are stacked directly on top of prefabricated photonic structures using pick-and-place assembly [18–21]. In this case, local strain arising from the nonplanar substrate, and spatially varying local dielectric screening result in a disordered energy landscape that perturbs the excitonic properties of 2D semiconductors [7,22]. While dielectric disorders can be partially mitigated by full hBN encapsulation [5–7], this

approach results in a trade-off between the strength of the disorder potential and the cavity-TMD coupling strength, by moving the TMD monolayer away from the antinode of the cavity field [21].

Besides improving the optical properties of TMDs, full hBN encapsulation also enhances the transport properties of excitons [5–7,23]. Indeed, markedly contrasting temperature dependencies of the exciton transport properties have been observed in hBN-encapsulated and bare TMD monolayers [24,25]. In quasi 0D nanocavities, exciton motion is expected to play an important role; light-matter couplings can enter the “nonlocal” regime [26] in which excitons sample different spatial regions of the cavity mode having dissimilar electric field amplitudes, during their lifetime. This is in strong contrast to the typical situation such as the III-V quantum dots, where the emitter size is much smaller than the emission wavelength and excitons are stationary, such that electric field is constant across the exciton wave function. In typical case, light-matter interaction is governed by the dipole approximation with a strength $\mathbf{d} \cdot \mathbf{E}(\mathbf{r})$ determined by the electron-hole dipole moment \mathbf{d} and the local electric field $\mathbf{E}(\mathbf{r})$ at the emitter position \mathbf{r} . In 2D materials, the c.m. motion of free excitons spatially extends over μm length scales [27], much larger than the emission wavelength. Therefore, $\mathbf{E}(\mathbf{r})$ is no longer constant during the exciton lifetime and the exciton-photon interaction enters the nonlocal regime [26,28]. Here, the light-matter

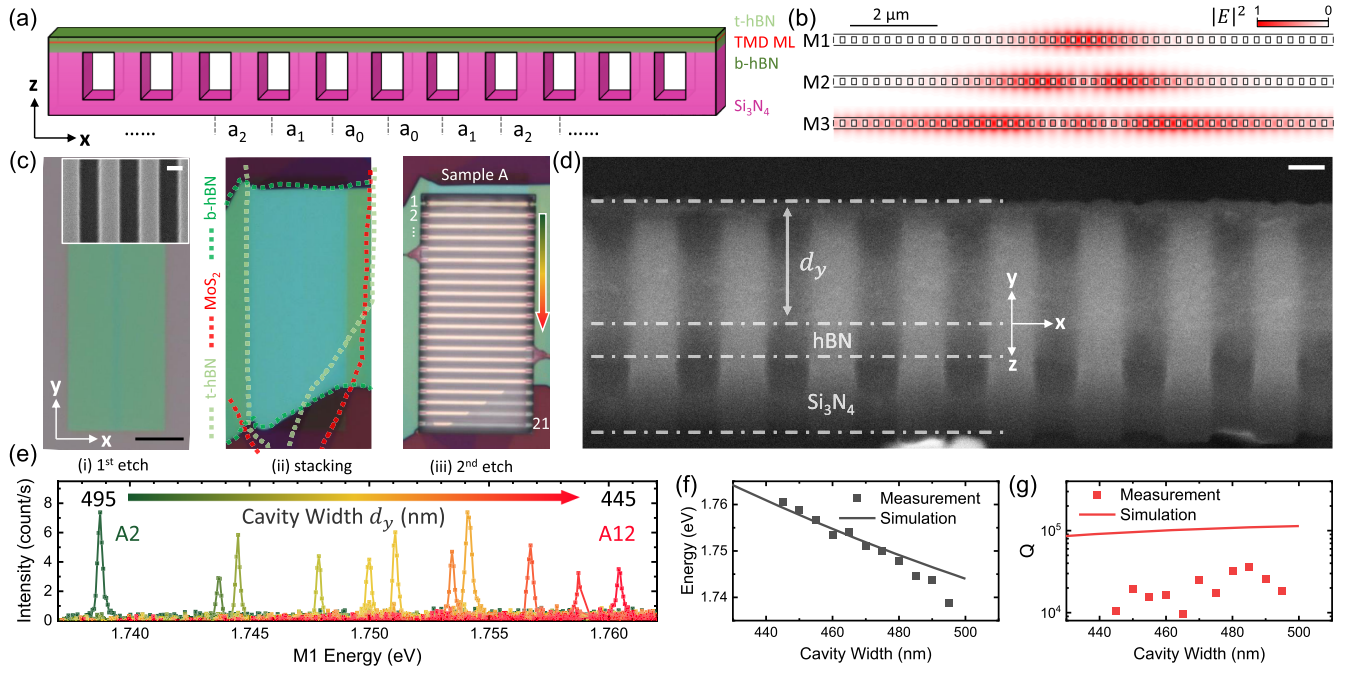


FIG. 1. (a) Schematic of cavity structures. (b) Maps of $|E|^2$ distribution of three modes M1–3. (c) Images of sample A with cavities A1–A21, recorded at different stages of the fabrication process: (i) after first etch (close up in inset), (ii) after stacking the TMD heterostructure, and (iii) following the second etch to define nanobeams. Here, the thickness of top (bottom) hBN is 15 (55) nm. (d) Image of one typical cavity (tilted 45°). (e) Room temperature PL spectra of cavities A2–A12 (arrow in (c)iii). (f),(g) Experimental and calculated cavity mode energy (f) and Q factors (g). The refractive indexes used in the calculation are $n_{\text{Si}_3\text{N}_4} = 2.00$ and $n_{\text{hBN}} = 1.82$. The black scale bar in (c) is $10 \mu\text{m}$ and the white scale bar in (c),(d) is 100 nm .

interaction is determined by an interplay in spatial between the cavity mode field and the c.m. wave function of the exciton [26].

Here, we observe nonlocal light-matter interactions in a hBN/MoS₂/hBN/Si₃N₄ hybrid photonic crystal nanocavities. Our optimized cavity structure solves the trade-off problem by integrating the hBN/MoS₂/hBN as a functional dielectric part of the cavity structure rather than an attachment. Therefore, the high excitonic quality and the strong cavity-MoS₂ overlap are achieved simultaneously. Our nanofabrication approach with encapsulated 2D materials provide cavity mode Q factors $\geq 10^4$, comparable to the best active III-V and silicon nanocavities explored for solid-state cQED experiments [29–31]. Optical spectroscopy performed as a function of lattice temperature shows that light-matter interactions between the cavity modes and spatially extended free trions (TXs) operate in the nonlocal regime [26,28]. The interaction strength is shown to be consistent with the shrinking c.m. wave function of TX as temperature increases. Our Letter demonstrates the significance of both optical and transport properties in hybrid 2D-material cQED systems, and the sensitivity of nonlocal effects to the environment. These results provide ways to the efficient control of exciton-photon interactions and enable hybrid 2D-material cQED systems for novel optoelectronic and quantum photonic devices.

The cavity structure is presented in Fig. 1(a) and the typical electric field distribution calculated using finite-difference time-domain methods for the first three modes (M1–M3) are presented in Fig. 1(b). Usually both the diameter of air holes and the periodicity decrease linearly in the cavity center for optimized nanobeam cavities [20,21]. Here, to simplify fabrication processes all nanoscale trenches were chosen to have the same width of 140 nm , but their separation a_i ($i \in 0, 1, 2, \dots$) follows a Gaussian function $a_i/a = 1 - A \cdot \exp[-i^2/(2\sigma^2)]$, where a is the lattice constant and $A = 0.1$, $\sigma = 4$ define a smoothly varying photon confinement for high Q factors [32].

The key fabrication steps are outlined in Fig. 1(c), where the images of sample A ($a = 270 \text{ nm}$) are presented with cavities marked by A_i ($i \in 1, 2, \dots$). Fabrication began by etching nanoscale trenches into Si₃N₄. Subsequently, large ($\geq 10^4 \mu\text{m}^2$) 2D flakes were exfoliated [33] before being assembled into a hBN/MoS₂/hBN heterostructure on top of the etched trenches using a viscoelastic dry transfer process [34]. The samples were completed in a second etching step that divides the heterostructure into multiple parallel nanocavity beams with a width d_y [Fig. 1(d)] that tunes the frequency of the cavity modes, followed by a final wet under-etch to produce freestanding nanobeams. The hBN/MoS₂/hBN heterostructure was only etched in the second etching and is not perforated, which retains

pristine excitonic properties of the MoS₂ monolayer and greatly reduces disorder-induced optical losses. Detailed design and fabrication is provided in the Supplemental Material [35].

Figure 1(e) shows typical photoluminescence (PL) spectra of the fundamental mode M1 from cavities A2–A12 with varying d_y . Luminescence from the MoS₂ filtered through the cavity mode is observed when exciting using a 532 nm constant wave laser. The laser spot area is 1 μm and the power density is 28.8 kW/cm². We observe cavity linewidths $\hbar\gamma_C \sim 200 \mu\text{eV}$, close to our resolution limit $\hbar\gamma_{\text{res}} = 130 \mu\text{eV}$. Thus the measurement of exact Q factors is limited by the spectral resolution. The Q factor estimated by deconvolution $Q = \omega_C/(\gamma_C - \gamma_{\text{res}})$ [59], where ω_C is the cavity mode frequency, are universally $\geq 10^4$ (for details, see the Supplemental Material [35]). These values are more than 1 order of magnitude larger than hBN cavities hitherto reported [60–62] and comparable to state-of-the-art III-V photonic crystal structures [29,30]. The observed functional dependence of the cavity energies and Q factors on the extensive geometry are in good accord with simulated results as shown in Figs. 1(f) and 1(g). The experimental Q factors are smaller than theoretical predictions due to the disorder in fabrication.

We continue by exploring the coupling between the MoS₂ monolayer and the fundamental M1 mode in our high- Q nanocavities. In all the cavities investigated, the emission from cavity mode could only be observed when M1 is “red detuned” from TX ($\Delta\omega = \omega_{\text{TX}} - \omega_{\text{M1}} \geq 0$). This can be clearly seen in Fig. 2, where the PL spectra is measured from cavities B1–B8 on another sample B [Fig. 2(a)], and from the cavity B2 where $\Delta\omega$ is mainly tuned via the temperature-dependent ω_{TX} [Fig. 2(b)]. The bare cavity mode is also slightly tuned by the temperature but much less compared to ω_{TX} (for full details, see the Supplemental Material [35]). In both sets of data, emission from the M1 mode quenches as $\Delta\omega < 0$. We note that this observation is distinct from previous studies of nonencapsulated monolayers attached to prefabricated nanocavities, where emission from cavity modes could be readily observed even when its energy is higher than the neutral exciton (X^0) [20]. We traced this phenomenon to the combined impact of reabsorption of cavity photons by the MoS₂ monolayer for long photon lifetimes (high Q) and the continuous energy spectrum of free excitons [63]. This differs significantly from the situation with discrete quantum emitters [63], such as quantum dots, due to the increased phase space of exciton states with nonzero momentum that can be accessed via inelastic scattering for blue detunings ($\Delta\omega < 0$). We estimate the impact of enhancing the photon lifetime in the high- Q cavity. Taking a typical absorption coefficient of $\alpha = 2.8 \times 10^4 \text{ m}^{-1}$ [64], we estimate that reabsorption of cavity photons by the MoS₂ becomes significant for $\alpha(Q/\omega_C)(c/n_r) \gg 1$ where Q/ω_C is the cavity photon lifetime, c is the speed of light,

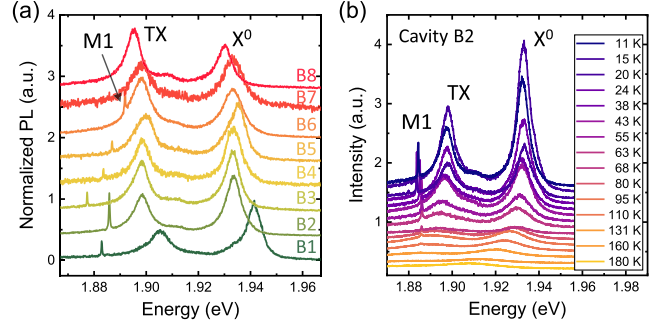


FIG. 2. (a) PL spectra recorded from sample B ($a = 250 \text{ nm}$) with cavities B1–B8 ($d_y = 530\text{--}460 \text{ nm}$) at 11 K. Excitation power is 1.4 kW/cm². Emission centered at 1.93 (1.90) eV is X^0 (TX). X^0 has a linewidth $\sim 5 \text{ meV}$, indicative of the high excitonic quality [6]. The sharp peaks on cavities B1–B6 at the red side of TX are the M1 modes. The nonmonotonic shift of M1 in B1–B2 reflects inhomogeneity of the hBN thickness. (b) Temperature-dependent PL spectra recorded from cavity B2 with excitation power 2.1 kW/cm². As T increases, the M1 peak intensity first continuously decreases as the exciton emission decreases, but then suddenly disappears after reaching the blue side of TX ($T > 131 \text{ K}$).

and n_r is the refractive index. For the maximum cavity-TMD overlap, we estimate $Q \gg 900$ to denote the limit beyond which reabsorption begins to limit the exciton-photon interaction. Our cavity Q exceeds this estimated threshold and, moreover, the MoS₂ monolayer is inserted close to the antinode of the cavity mode. Thus, the cavity mode quenches for blue detunings $\Delta\omega < 0$.

To analyze the coupling of TXs to the high- Q cavity mode, we extracted the peak energy and linewidth of the cavity mode and TX from the spectra in Fig. 2(b) by multi-Lorentz fitting, e.g., the spectra at 95 K presented in Fig. 3(a). Since the interaction is at low excitation level without nonlinearity (for full details, see the Supplemental Material [35]), the Jaynes-Cummings model is used to model the cavity-TX interaction [21]. Hereby, when the cavity-TX interaction is weak, the interaction strength g can be calculated from the linewidth of cavitylike polariton γ_- , the energy detuning ($\Delta\omega'$), and linewidth difference ($\Delta\gamma'$) between the excitonlike and cavitylike polariton branch by $\gamma_- = \gamma_C + g^2\Delta\gamma'/(\Delta\omega'^2 + 1/4\Delta\gamma'^2)$. The experimental extracted parameters are presented in Figs. 3(b) and 3(c), and the results of g are summarized in Fig. 3(d) as the central results of this Letter. First, the values of g are far smaller than that expected of a strong coupling; thus, the small g approximation in the calculation is right. Furthermore, the experimentally determined g (black dots) is found to be highly nonmonotonic as the temperature T increases (detuning reduces): g first *reduces* with increasing T before *increasing* rapidly—a behavior that can be accounted for by nonlocal light-matter interactions of mobile excitons in the hybrid nanocavity [26,28]. This situation can occur, e.g., for plasmonic systems with tightly

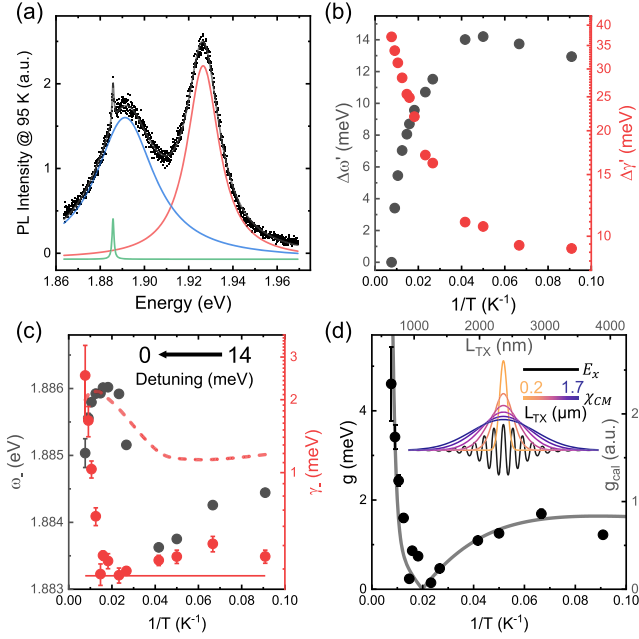


FIG. 3. (a) PL spectra at 95 K and the multi-Lorentz fitting. (b) $\Delta\omega'$ and $\Delta\gamma'$ extracted from experimental data. (c) ω_- (energy of the cavity-branch peak) and γ_- . Red solid line is the bare cavity linewidth γ_C . Red dashed line is the γ_- predicted with a constant interaction strength g' . (d) Results of interaction strength g . Points are experimentally extracted at different temperatures. The solid line shows theoretical results calculated with the cavity electric field E_x from mode M1 and the c.m. wave packet χ_{CM} with different spatial extent L_{TX} presented in the inset.

confined electromagnetic modes [65–67] or in situations where the exciton wave function has a large spatial extent, e.g., large quantum dots [68]. Additionally, it can be observed that the γ_- predicted by a constant g' of 4 meV [red dashed line in Fig. 3(c)] is clearly different to the experimental observation; thus, a constant g' is obviously not our case.

We continue to explain how this behavior is expected in the nonlocal regime of light-matter interactions. In the local regime, $\mathbf{E}(\mathbf{r})$, which usually involves $e^{i\mathbf{k}\cdot\mathbf{r}}$ (\mathbf{k} is the wave vector), is approximately constant within the exciton wave function. This translates to $\mathbf{k}\cdot\mathbf{r} \ll 1$ for all \mathbf{r} within the electron and hole wave functions, whereas nonlocal regime occurs when $\mathbf{k}\cdot\mathbf{r}$ is non-negligible [26,28,68]. The free excitons in the hBN-encapsulated MoS₂ are generated locally but their c.m. samples' positions having different local cavity field ($\mathbf{k}\cdot\mathbf{r} \gg 1$) before recombining. Hereby, TXs were modeled in the weak confinement regime (effective Bohr radius \ll the spatial extent of the c.m. wave function) for which the total wave function is separable into components arising from the c.m. motion $\chi_{CM}(\mathbf{R})$ and internal dynamics of the e - h pair $\chi_{rel}(\mathbf{r}')$, respectively. $\mathbf{R} = (m_e\mathbf{r}_e + m_h\mathbf{r}_h)/(m_e + m_h)$ corresponds to the c.m. motion and $\mathbf{r}' = \mathbf{r}_e - \mathbf{r}_h$ accounts for the internal relative motion of the e - h pair [4,26]. Because of the

large exciton binding energy in hBN-encapsulated TMDs [3,4,69], $\chi_{rel}(\mathbf{r}')$ only extends over a few nanometers [1,4]. Moreover, it is expected to be fully independent of temperature since the exciton binding energy is $\gg k_B \cdot T$. In contrast, due to exciton-phonon coupling, the spatial extent of the c.m. wave function has a negative temperature relation in hBN-encapsulated TMDs [24,25,70]. Generally acoustic photons result in L_{TX} that varies sublinearly with $1/T$, while optical phonons result in L_{TX} that varies superlinearly [71]. We performed calculations using a Gaussian wave packet to describe the c.m. motion $\chi_{CM}(x) = (1/\pi)^{1/4}(1/L_{TX})^{1/2}e^{-x^2/2L_{TX}^2}$ [26], and considered the spatial extent L_{TX} following a $1/T$ dependence (colored lines in Fig. 3(d) inset). As the unit cell in MoS₂ (~ 0.3 nm) is much smaller than the TX emission wavelength, the interaction strength is $g_{cal} = |\int \chi_{CM}(x)E_x(x)dx|$ [26], where $E_x(x)$ is the cavity electric field of mode M1 (black line in Fig. 3(d) inset). The resulting L dependence of g_{cal} is presented by the gray line in Fig. 3(d) and reproduces our experimental findings (dots) remarkably well, despite the simplicity of our model. Therefore, the nontrivial temperature dependence of cavity-TX interaction are best reproduced by the nonlocal light-matter interaction physics. At $T = 300$ K, the corresponding L_{TX} is 480 ± 30 nm. Considering the nondegenerate single optical mode in the cavity is spatially coherent, and the enhancement by hBN encapsulation and Si₃N₄ stress [24,72,73], this value of L_{TX} close to the recently reported diffusion length of 300 nm is a reasonable result [27]. Here, we note that the extent of the c.m. wave function and the exciton diffusion length both describe the spatial distribution of excitons. However, they are not strictly equivalent since the exciton diffusion length also includes inelastic scattering processes. The theoretical analysis used here is based on the c.m. wave function that is not necessarily equal to the diffusion length. Thus, any distinction does not have any substantive impact on the conclusions drawn from Fig. 3.

Other factors such as gas condensation and localized excitons are unlikely to explain the nonmonotonic g since they have very little affect on the cavity polariton linewidth (for details, see the Supplemental Material [35]). In addition, we note that the c.m. wave function $\chi_{CM}(\mathbf{R})$ is *not* equivalent to a Gaussian spatial distribution of excitons $\chi_{CM}^2(x)$. In the latter case, the interaction strength would be $g_{cal}^2 = \int \chi_{CM}^2(x)E_x^2(x)dx$ corresponding to a monotonic decreasing g as L increases (for details, see the Supplemental Material [35]). Conversely, here $E_x(x)$ has both positive and negative values depending on the position x , and thus the integral $\int \chi_{CM}(x)E_x(x)dx$ has both positive and negative contributions, resulting in the minimum interaction strength for specific constellations, such as when $L_{TX} = 1.1 \mu\text{m}$ around twice the wavelength of the cavity electric field in Fig. 3(d).

In summary, we explored novel light-matter interaction regimes of free trions in a hybrid high- Q photonic crystal

nanocavity embedded with pristine hBN/TMD/hBN heterostructures. The optimized structure provided quasi 0D modes with $Q > 10^4$, exciton linewidths of MoS₂ approaching homogeneous limit and large cavity-MoS₂ overlap. These advances facilitated the demonstration of nonlocal interaction between the cavity and free trions. Since our approaches can be applied to any 2D materials, our Letter provides an ideal platform to investigate cQED and quantum photonics using 2D materials. Therefore, additional interesting phenomena could be expected in future work, e.g., the interaction with site-selectively generated defects [74] or Moiré exciton lattices [75,76], toward highly scalable quantum photonic devices.

All authors gratefully acknowledge the German Science Foundation (DFG) for financial support via Grants No. FI 947/8-1, DI 2013/5-1, and SPP-2244, as well as the clusters of excellence MCQST (EXS-2111) and e-conversion (EXS-2089). C. Q. and V. V. gratefully acknowledge the Alexander von Humboldt Foundation for financial support in the framework of their fellowship program. K. W. and T. T. acknowledge support from the Elemental Strategy Initiative conducted by the MEXT, Japan (Grant No. JPMXP0112101001) and JSPS KAKENHI (Grants No. 19H05790 and JP20H00354).

*Corresponding author.

chenjiang.qian@wsi.tum.de

†Corresponding author.

finley@wsi.tum.de

- [1] G. Wang, A. Chernikov, M. M. Glazov, T. F. Heinz, X. Marie, T. Amand, and B. Urbaszek, Colloquium: Excitons in atomically thin transition metal dichalcogenides, *Rev. Mod. Phys.* **90**, 021001 (2018).
- [2] V. Ardizzone, L. D. Marco, M. D. Giorgi, L. Dominici, D. Ballarini, and D. Sanvitto, Emerging 2D materials for room-temperature polaritonics, *Nanophotonics* **8**, 1547 (2019).
- [3] A. V. Stier, N. P. Wilson, K. A. Velizhanin, J. Kono, X. Xu, and S. A. Crooker, Magneto-optics of Exciton Rydberg States in a Monolayer Semiconductor, *Phys. Rev. Lett.* **120**, 057405 (2018).
- [4] M. Goryca, J. Li, A. V. Stier, T. Taniguchi, K. Watanabe, E. Courtade, S. Shree, C. Robert, B. Urbaszek, X. Marie, and S. A. Crooker, Revealing exciton masses and dielectric properties of monolayer semiconductors with high magnetic fields, *Nat. Commun.* **10**, 4172 (2019).
- [5] J. Wierzbowski, J. Klein, F. Sigger, C. Straubinger, M. Kremser, T. Taniguchi, K. Watanabe, U. Wurstbauer, A. W. Holleitner, M. Kaniber, K. Müller, and J. J. Finley, Direct exciton emission from atomically thin transition metal dichalcogenide heterostructures near the lifetime limit, *Sci. Rep.* **7**, 12383 (2017).
- [6] F. Cadiz, E. Courtade, C. Robert, G. Wang, Y. Shen, H. Cai, T. Taniguchi, K. Watanabe, H. Carrere, D. Lagarde, M. Manca, T. Amand, P. Renucci, S. Tongay, X. Marie, and B. Urbaszek, Excitonic Linewidth Approaching the Homogeneous Limit in MoS₂-Based van der Waals Heterostructures, *Phys. Rev. X* **7**, 021026 (2017).
- [7] A. Raja, L. Waldecker, J. Zipfel, Y. Cho, S. Brem, J. D. Ziegler, M. Kulig, T. Taniguchi, K. Watanabe, E. Malic, T. F. Heinz, T. C. Berkelbach, and A. Chernikov, Dielectric disorder in two-dimensional materials, *Nat. Nanotechnol.* **14**, 832 (2019).
- [8] Y. Li, A. Chernikov, X. Zhang, A. Rigosi, H. M. Hill, A. M. van der Zande, D. A. Chenet, E.-M. Shih, J. Hone, and T. F. Heinz, Measurement of the optical dielectric function of monolayer transition-metal dichalcogenides: MoS₂, MoSe₂, WS₂, and WSe₂, *Phys. Rev. B* **90**, 205422 (2014).
- [9] A. Castellanos-Gomez, M. Buscema, R. Molenaar, V. Singh, L. Janssen, H. S. J. v. d. Zant, and G. A. Steele, Deterministic transfer of two-dimensional materials by all-dry viscoelastic stamping, *2D Mater.* **1**, 011002 (2014).
- [10] C. Schneider, M. M. Glazov, T. Korn, S. Hfling, and B. Urbaszek, Two-dimensional semiconductors in the regime of strong light-matter coupling, *Nat. Commun.* **9**, 2695 (2018).
- [11] S. Dufferwiel, S. Schwarz, F. Withers, A. A. P. Trichet, F. Li, M. Sich, O. D. Pozo-Zamudio, C. Clark, A. Nalitov, D. D. Solnyshkov, G. Malpuech, K. S. Novoselov, J. M. Smith, M. S. Skolnick, D. N. Krizhanovskii, and A. I. Tartakovskii, Exciton polaritons in van der Waals heterostructures embedded in tunable microcavities, *Nat. Commun.* **6**, 8579 (2015).
- [12] L. Zhang, R. Gogna, W. Burg, E. Tutuc, and H. Deng, Photonic-crystal exciton-polaritons in monolayer semiconductors, *Nat. Commun.* **9**, 713 (2018).
- [13] X. Ma, N. Youngblood, X. Liu, Y. Cheng, P. Cunha, K. Kudtarkar, X. Wang, and S. Lan, Engineering photonic environments for two-dimensional materials, *Nanophotonics* **10**, 1031 (2020).
- [14] D. Rosser, D. Gerace, L. C. Andreani, and A. Majumdar, Optimal condition to probe strong coupling of two-dimensional excitons and zero-dimensional cavity modes, *Phys. Rev. B* **104**, 235436 (2021).
- [15] N. Lundt, A. Maryński, E. Cherotchenko, A. Pant, X. Fan, S. Tongay, G. Sek, A. V. Kavokin, S. Hfling, and C. Schneider, Monolayered MoSe₂: A candidate for room temperature polaritonics, *2D Mater.* **4**, 015006 (2016).
- [16] T. Hu, Y. Wang, L. Wu, L. Zhang, Y. Shan, J. Lu, J. Wang, S. Luo, Z. Zhang, L. Liao, S. Wu, X. Shen, and Z. Chen, Strong coupling between Tamm plasmon polariton and two dimensional semiconductor excitons, *Appl. Phys. Lett.* **110**, 051101 (2017).
- [17] L. C. Flatten, Z. He, D. M. Coles, A. A. P. Trichet, A. W. Powell, R. A. Taylor, J. H. Warner, and J. M. Smith, Room-temperature exciton-polaritons with two-dimensional WS₂, *Sci. Rep.* **6**, 33134 (2016).
- [18] S. Wu, S. Buckley, J. R. Schaibley, L. Feng, J. Yan, D. G. Mandrus, F. Hatami, W. Yao, J. Vučković, A. Majumdar, and X. Xu, Monolayer semiconductor nanocavity lasers with ultralow thresholds, *Nature (London)* **520**, 69 (2015).
- [19] Y. Ye, Z. J. Wong, X. Lu, X. Ni, H. Zhu, X. Chen, Y. Wang, and X. Zhang, Monolayer excitonic laser, *Nat. Photonics* **9**, 733 (2015).
- [20] Y. Li, J. Zhang, D. Huang, H. Sun, F. Fan, J. Feng, Z. Wang, and C. Z. Ning, Room-temperature continuous-wave lasing

- from monolayer molybdenum ditelluride integrated with a silicon nanobeam cavity, *Nat. Nanotechnol.* **12**, 987 (2017).
- [21] D. Rosser, D. Gerace, Y. Chen, Y. Liu, J. Whitehead, A. Ryou, L. C. Andreani, and A. Majumdar, Dispersive coupling between MoSe₂ and an integrated zero-dimensional nanocavity, *Opt. Mater. Express* **12**, 59 (2022).
- [22] D. Rhodes, S. H. Chae, R. Ribeiro-Palau, and J. Hone, Disorder in van der Waals heterostructures of 2D materials, *Nat. Mater.* **18**, 541 (2019).
- [23] L. Ju, J. Velasco, E. Huang, S. Kahn, C. Nosiola, H.-Z. Tsai, W. Yang, T. Taniguchi, K. Watanabe, Y. Zhang, G. Zhang, M. Crommie, A. Zettl, and F. Wang, Photoinduced doping in heterostructures of graphene and boron nitride, *Nat. Nanotechnol.* **9**, 348 (2014).
- [24] R. Rosati, R. Perea-Causn, S. Brem, and E. Malic, Negative effective excitonic diffusion in monolayer transition metal dichalcogenides, *Nanoscale* **12**, 356 (2020).
- [25] T. Kato and T. Kaneko, Transport dynamics of neutral excitons and trions in monolayer WS₂, *ACS Nano* **10**, 9687 (2016).
- [26] S. Stobbe, P. T. Kristensen, J. E. Mortensen, J. M. Hvam, J. Mørk, and P. Lodahl, Spontaneous emission from large quantum dots in nanostructures: Exciton-photon interaction beyond the dipole approximation, *Phys. Rev. B* **86**, 085304 (2012).
- [27] S. Z. Uddin, H. Kim, M. Lorenzon, M. Yeh, D.-H. Lien, E. S. Barnard, H. Htoon, A. Weber-Bargioni, and A. Javey, Neutral exciton diffusion in monolayer MoS₂, *ACS Nano* **14**, 13433 (2020).
- [28] C. Qian, X. Xie, J. Yang, and X. Xu, A cratered photonic crystal cavity mode for non-local exciton photon interactions, *Adv. Quantum Technol.* **3**, 1900024 (2020).
- [29] T. Yoshie, A. Scherer, J. Hendrickson, G. Khitrova, H. M. Gibbs, G. Rupper, C. Ell, O. B. Shchekin, and D. G. Deppe, Vacuum Rabi splitting with a single quantum dot in a photonic crystal nanocavity, *Nature (London)* **432**, 200 (2004).
- [30] K. Hennessy, A. Badolato, M. Winger, D. Gerace, M. Atatüre, S. Gulde, S. Fält, E. L. Hu, and A. Imamoglu, Quantum nature of a strongly coupled single quantum dot-cavity system, *Nature (London)* **445**, 896 (2007).
- [31] A. Shaloor, R. Lo Savio, P. Cardile, S. L. Portalupi, D. Gerace, K. Welna, S. Boninelli, G. Franz, F. Priolo, T. F. Krauss, M. Galli, and L. O'Faolain, Room temperature all-silicon photonic crystal nanocavity light emitting diode at sub-bandgap wavelengths, *Laser Photonics Rev.* **7**, 114 (2013).
- [32] Y. Akahane, T. Asano, B.-S. Song, and S. Noda, High-Q photonic nanocavity in a two-dimensional photonic crystal, *Nature (London)* **425**, 944 (2003).
- [33] Z. Huang, A. Alharbi, W. Mayer, E. Cuniberto, T. Taniguchi, K. Watanabe, J. Shabani, and D. Shahrjerdi, Versatile construction of van der Waals heterostructures using a dual-function polymeric film, *Nat. Commun.* **11**, 3029 (2020).
- [34] F. Pizzocchero, L. Gammelgaard, B. S. Jessen, J. M. Caridad, L. Wang, J. Hone, P. Bøggild, and T. J. Booth, The hot pick-up technique for batch assembly of van der Waals heterostructures, *Nat. Commun.* **7**, 11894 (2016).
- [35] See Supplemental Material at <http://link.aps.org/supplemental/10.1103/PhysRevLett.128.237403> for the detailed information on nanocavity design, fabrication methods, and additional results, which includes Refs. [36–58].
- [36] S. Grenadier, J. Li, J. Lin, and H. Jiang, Dry etching techniques for active devices based on hexagonal boron nitride epilayers, *J. Vac. Sci. Technol. A* **31**, 061517 (2013).
- [37] J. D. Caldwell, A. V. Kretinin, Y. Chen, V. Giannini, M. M. Fogler, Y. Francescato, C. T. Ellis, J. G. Tischler, C. R. Woods, A. J. Giles, M. Hong, K. Watanabe, T. Taniguchi, S. A. Maier, and K. S. Novoselov, Sub-diffractive volume-confined polaritons in the natural hyperbolic material hexagonal boron nitride, *Nat. Commun.* **5**, 5221 (2014).
- [38] A. Jain, P. Bharadwaj, S. Heeg, M. Parzefall, T. Taniguchi, K. Watanabe, and L. Novotny, Minimizing residues and strain in 2d materials transferred from PDMS, *Nanotechnology* **29**, 265203 (2018).
- [39] S. Shree, A. George, T. Lehnert, C. Neumann, M. Benelajla, C. Robert, X. Marie, K. Watanabe, T. Taniguchi, U. Kaiser, B. Urbaszek, and A. Turchanin, High optical quality of MoS₂ monolayers grown by chemical vapor deposition, *2D Mater.* **7**, 015011 (2019).
- [40] S.-Y. Lee, T.-Y. Jeong, S. Jung, and K.-J. Yee, Refractive index dispersion of hexagonal boron nitride in the visible and near-infrared, *Phys. Status Solidi B* **256**, 1800417 (2019).
- [41] Y. Rah, Y. Jin, S. Kim, and K. Yu, Optical analysis of the refractive index and birefringence of hexagonal boron nitride from the visible to near-infrared, *Opt. Lett.* **44**, 3797 (2019).
- [42] Y. Zhou, G. Scuri, D. S. Wild, A. A. High, A. Dibos, L. A. Jauregui, C. Shu, K. De Greve, K. Pistunova, A. Y. Joe, T. Taniguchi, K. Watanabe, P. Kim, M. D. Lukin, and H. Park, Probing dark excitons in atomically thin semiconductors via near-field coupling to surface plasmon polaritons, *Nat. Nanotechnol.* **12**, 856 (2017).
- [43] P. Rivera, H. Yu, K. L. Seyler, N. P. Wilson, W. Yao, and X. Xu, Interlayer valley excitons in heterobilayers of transition metal dichalcogenides, *Nat. Nanotechnol.* **13**, 1004 (2018).
- [44] D. Golla, K. Chattrakun, K. Watanabe, T. Taniguchi, B. J. LeRoy, and A. Sandhu, Optical thickness determination of hexagonal boron nitride flakes, *Appl. Phys. Lett.* **102**, 161906 (2013).
- [45] M. G. Stanford, P. D. Rack, and D. Jariwala, Emerging nanofabrication and quantum confinement techniques for 2d materials beyond graphene, *npj 2D Mater. Appl.* **2**, 20 (2018).
- [46] T. P. Lyons, S. Dufferwiel, M. Brooks, F. Withers, T. Taniguchi, K. Watanabe, K. S. Novoselov, G. Burkard, and A. I. Tartakovskii, The valley Zeeman effect in inter- and intra-valley trions in monolayer WSe₂, *Nat. Commun.* **10**, 2330 (2019).
- [47] S. Mosor, J. Hendrickson, B. C. Richards, J. Sweet, G. Khitrova, H. M. Gibbs, T. Yoshie, A. Scherer, O. B. Shchekin, and D. G. Deppe, Scanning a photonic crystal slab nanocavity by condensation of xenon, *Appl. Phys. Lett.* **87**, 141105 (2005).
- [48] A. W. Elshaari, I. E. Zadeh, K. D. Jns, and V. Zwiller, Thermo-optic characterization of silicon nitride resonators

- for cryogenic photonic circuits, *IEEE Photonics J.* **8**, 1 (2016).
- [49] S. Takayoshi, W. Kokuyama, and H. Fukuyama, The boiling suppression of liquid nitrogen, *Cryogenics* **49**, 221 (2009).
- [50] A. Witkowski, M. Majkut, and S. Rulik, Analysis of pipeline transportation systems for carbon dioxide sequestration, *Arch. Thermodyn.* **35**, 117 (2014).
- [51] K. Greben, S. Arora, M. G. Harats, and K. I. Bolotin, Intrinsic and extrinsic defect-related excitons in TMDCs, *Nano Lett.* **20**, 2544 (2020).
- [52] M. He, P. Rivera, D. Van Tuan, N. P. Wilson, M. Yang, T. Taniguchi, K. Watanabe, J. Yan, D. G. Mandrus, H. Yu, H. Dery, W. Yao, and X. Xu, Valley phonons and exciton complexes in a monolayer semiconductor, *Nat. Commun.* **11**, 618 (2020).
- [53] M. Barbone, A. R.-P. Montblanch, D. M. Kara, C. Palacios-Berraquero, A. R. Cadore, D. De Fazio, B. Pingault, E. Mostaani, H. Li, B. Chen, K. Watanabe, T. Taniguchi, S. Tongay, G. Wang, A. C. Ferrari, and M. Atatüre, Charge-tunable biexciton complexes in monolayer WSe₂, *Nat. Commun.* **9**, 3721 (2018).
- [54] J. Lee, Z. Wang, H. Xie, K. F. Mak, and J. Shan, Valley magnetoelectricity in single-layer MoS, *Nat. Mater.* **16**, 887 (2017).
- [55] D. Ge, Y. Zhang, H. Chen, G. Zhen, M. Wang, J. Jiao, L. Zhang, and S. Zhu, Effect of patterned silicon nitride substrate on Raman scattering and stress of graphene, *Mater. Des.* **198**, 109338 (2021).
- [56] J. Zhang, L. Ding, S. Zhou, Y. M. Xiao, and W. Xu, Observation and optical control of saturable excitonic behaviors in monolayer MoS₂, *Phys. Status Solidi RRL* **14**, 2000222 (2020).
- [57] M. Radulaski, K. A. Fischer, K. G. Lagoudakis, J. L. Zhang, and J. Vučković, Photon blockade in two-emitter-cavity systems, *Phys. Rev. A* **96**, 011801(R) (2017).
- [58] Y. Kangawa, T. Ito, A. Taguchi, K. Shiraishi, T. Irisawa, and T. Ohachi, Monte Carlo simulation for temperature dependence of Ga diffusion length on GaAs (0 0 1), *Appl. Surf. Sci.* **190**, 517 (2002).
- [59] J. Jimenez-Mier, Contribution of the instrument window function to the profile of autoionizing resonances, *J. Quant. Spectrosc. Radiat. Transfer* **51**, 741 (1994).
- [60] S. Kim, J. E. Fröch, J. Christian, M. Straw, J. Bishop, D. Totonjian, K. Watanabe, T. Taniguchi, M. Toth, and I. Aharonovich, Photonic crystal cavities from hexagonal boron nitride, *Nat. Commun.* **9**, 2623 (2018).
- [61] J. E. Frch, Y. Hwang, S. Kim, I. Aharonovich, and M. Toth, Photonic nanostructures from hexagonal boron nitride, *Adv. Opt. Mater.* **7**, 1801344 (2019).
- [62] J. E. Frch, S. Kim, N. Mendelson, M. Kianinia, M. Toth, and I. Aharonovich, Coupling hexagonal boron nitride quantum emitters to photonic crystal cavities, *ACS Nano* **14**, 7085 (2020).
- [63] W. J. Parak, L. Manna, and T. Nann, Fundamental principles of quantum dots, in *Nanotechnology* (Wiley-VCH, Weinheim, 2010), Chap. 4, pp. 73–96, 10.1002/9783527628155.
- [64] J. Y. Kwak, Absorption coefficient estimation of thin MoS₂ film using attenuation of silicon substrate Raman signal, *Results Phys.* **13**, 102202 (2019).
- [65] M. L. Andersen, S. Stobbe, A. S. Sørensen, and P. Lodahl, Strongly modified plasmon–matter interaction with mesoscopic quantum emitters, *Nat. Phys.* **7**, 215 (2011).
- [66] E. J. C. Dias, D. A. Iranzo, P. A. D. Goneçalves, Y. Hajati, Y. V. Bludov, A.-P. Jauho, N. A. Mortensen, F. H. L. Koppens, and N. M. R. Peres, Probing nonlocal effects in metals with graphene plasmons, *Phys. Rev. B* **97**, 245405 (2018).
- [67] D. Alcaraz Iranzo, S. Nanot, E. J. C. Dias, I. Epstein, C. Peng, D. K. Efetov, M. B. Lundeberg, R. Parret, J. Osmond, J.-Y. Hong, J. Kong, D. R. Englund, N. M. R. Peres, and F. H. L. Koppens, Probing the ultimate plasmon confinement limits with a van der waals heterostructure, *Science* **360**, 291 (2018).
- [68] C. Qian, X. Xie, J. Yang, K. Peng, S. Wu, F. Song, S. Sun, J. Dang, Y. Yu, M. J. Steer, I. G. Thayne, K. Jin, C. Gu, and X. Xu, Enhanced Strong Interaction between Nanocavities and *p*-shell Excitons Beyond the Dipole Approximation, *Phys. Rev. Lett.* **122**, 087401 (2019).
- [69] A. V. Stier, N. P. Wilson, G. Clark, X. Xu, and S. A. Crooker, Probing the influence of dielectric environment on excitons in monolayer WSe₂: Insight from high magnetic fields, *Nano Lett.* **16**, 7054 (2016).
- [70] H. Wang, C. Zhang, W. Chan, C. Manolatu, S. Tiwari, and F. Rana, Radiative lifetimes of excitons and trions in monolayers of the metal dichalcogenide MoS₂, *Phys. Rev. B* **93**, 045407 (2016).
- [71] N. Zinovev, L. Ivanov, I. Lang, S. Pavlov, A. Prokaznikov, and I. Yaroshetskii, Exciton diffusion and the mechanism of exciton momentum scattering in semiconductors, *Sov. Phys. JETP* **57**, 1254 (1983), http://www.jetp.ras.ru/cgi-bin/dn/e_057_06_1254.pdf.
- [72] Y. Chai, S. Su, D. Yan, M. Ozkan, R. Lake, and C. S. Ozkan, Strain gated bilayer molybdenum disulfide field effect transistor with edge contacts, *Sci. Rep.* **7**, 41593 (2017).
- [73] A. P. John, A. Thenappambil, and M. Thalukulam, Strain-engineering the Schottky barrier and electrical transport on MoS₂, *Nanotechnology* **31**, 275703 (2020).
- [74] J. Klein, M. Lorke, M. Florian, F. Sigger, L. Sigl, S. Rey, J. Wierzbowski, J. Cerne, K. Müller, E. Mitterreiter, P. Zimmermann, T. Taniguchi, K. Watanabe, U. Wurstbauer, M. Kaniber, M. Knap, R. Schmidt, J. J. Finley, and A. W. Holleitner, Site-selectively generated photon emitters in monolayer MoS₂ via local helium ion irradiation, *Nat. Commun.* **10**, 2755 (2019).
- [75] K. L. Seyler, P. Rivera, H. Yu, N. P. Wilson, E. L. Ray, D. G. Mandrus, J. Yan, W. Yao, and X. Xu, Signatures of moiré-trapped valley excitons in MoSe₂/WSe₂ heterobilayers, *Nature (London)* **567**, 66 (2019).
- [76] H. Baek, M. Brotons-Gisbert, Z. X. Koong, A. Campbell, M. Rambach, K. Watanabe, T. Taniguchi, and B. D. Gerardot, Highly energy-tunable quantum light from moiré-trapped excitons, *Sci. Adv.* **6**, eaba8526 (2020).